Journal of Rock Mechanics and Geotechnical Engineering xxx (2017) 1–10

Contents lists available at ScienceDirect

Journal of Rock Mechanics and Geotechnical Engineering

journal homepage: www.rockgeotech.org

Full Length Article

Analysis of rockburst in tunnels subjected to static and dynamic loads

Amin Manouchehrian [a,b], Ming Cai [a,b,c,*]

[a] Bharti School of Engineering, Laurentian University, Sudbury, P3E 2C6, Canada
[b] MIRARCO, Laurentian University, 935 Ramsey Lake Road, Sudbury P3E 2C6, Canada
[c] State Key Laboratory of Geomechanics and Geotechnical Engineering, Institute of Rock and Soil Mechanics, Chinese Academy of Sciences, Wuhan, 430071, Hubei, China

ARTICLE INFO

Article history:
Received 11 January 2017
Received in revised form
25 June 2017
Accepted 26 July 2017
Available online xxx

Keywords:
Rockburst
Numerical modeling
Geological structure
Static load increase
Dynamic disturbance
Tunnel

ABSTRACT

The presence of geological structures such as faults, joints, and dykes has been observed near excavation boundaries in many rockburst case histories. In this paper, the role of discontinuities around tunnels in rockburst occurrence was studied. For this purpose, the Abaqus explicit code was used to simulate dynamic rock failure in deep tunnels. Material heterogeneity was considered using Python scripting in Abaqus. Rockbursts near fault regions in deep tunnels under static and dynamic loads were studied. Several tunnel models with and without faults were built and static and dynamic loads were used to simulate rock failure. The velocity and the released kinetic energy of failed rocks, the failure zone around the tunnel, and the deformed mesh were studied to identify stable and unstable rock failures. Compared with models without discontinuities, the results showed that the velocity and the released kinetic energy of failed rocks were higher, the failure zone around the tunnel was larger, and the mesh was more deformed in the models with discontinuities, indicating that rock failure in the models with discontinuities was more violent. The modeling results confirm that the presence of geological structures in the vicinity of deep excavations could be one of the major influence factors for the occurrence of rockburst. It can explain localized rockburst occurrence in civil tunnels and mining drifts. The presented methodology in this paper for rockburst analysis can be useful for rockburst anticipation and control during mining and tunneling in highly stressed ground.

1. Introduction

Mankind's life is very dependent on the Earth's materials. Continuous mining over the past years has depleted most surface and shallow reserves and forced us to go deeper inside the Earth for more natural resources. Mining conditions are difficult in deep grounds; it is harder and more risky to mine at depth. One of engineering hazards of mining at depth is rockburst. A rockburst is an unstable failure of rock associated with a sudden release of energy, and it imposes a great danger on the safety of workers and investment.

Case histories in mining have documented violent rock failures that were accompanied by rapid ejection of debris and broken rocks into working areas of mine openings and tunnels (Shepherd et al., 1981; Ghose and Rao, 1990; Hedley, 1992; Young, 1993; Gibowicz and Lasocki, 1997; Blake and Hedley, 2003; Zhang et al., 2012; Andrieux et al., 2013). In some cases, these violent unstable failures have resulted in loss of life and total collapse of mine panels (Chen et al., 1997; Whyatt et al., 2002; Zhu et al., 2009; Zhang et al., 2013). Violent rock failure can occur locally in isolation, which may not affect the general stability of a mine, but poses a great threat to personnel in the area. Modern mining operations take available measures to reduce the likelihood of unstable rock failures, but complete elimination of unstable rock failures is difficult in practice due to the uncertainty in rock stress, strength, stiffness, and other mechanical properties (Cai, 2013). Over the past five decades, researchers have studied unstable rock failure and rockbursting using various means such as analytical, numerical, experimental, and statistical approaches (Sun et al., 2007; He et al., 2010, 2012; Li et al., 2012, 2013, 2014; Tao et al., 2012; Zhu et al., 2014; Zhao and Cai, 2014; Xiao et al., 2016). However, many conditions leading to rockburst occurrence are not fully understood and further studies are needed to understand the mechanisms of rockbursting so as to control and mitigate rockburst risk.

* Corresponding author.
E-mail address: mcai@laurentian.ca (M. Cai).

Peer review under responsibility of Institute of Rock and Soil Mechanics, Chinese Academy of Sciences.

https://doi.org/10.1016/j.jrmge.2017.07.001

Ortlepp (1997) classified rockbursts into five types (strainburst, buckling, face crush/pillar burst, shear rupture, and fault-slip burst). In a broad sense, they can be grouped into three rockburst types, i.e. strainburst, pillar burst, and fault-slip burst. Strainbursts, which are due to stress concentration and strain energy accumulation and release, can be assessed based on stress or energy consideration (Mitri et al., 1999). Pillar bursts can be assessed by comparison of local mine stiffness to pillar's post-peak stiffness (Zipf, 1996). Fault-slip bursts, which are larger seismic events in general, can be assessed based on potential movement (slip) of the fault, slip rate, and seismic moment (Sainoki and Mitri, 2014).

Rockburst case histories reveal that rockburst damage is often localized and not uniform. In other words, the damage extent in a tunnel caused by a rockburst varies at different locations. The localized rockburst damage originates from the complex mechanisms that drive rockbursts and the contribution of influence factors on rockburst occurrence. Many factors influencing rockburst damages have been identified, but no one knows the exact condition for the occurrence of a rockburst in a complex underground setting (Kaiser and Cai, 2012).

It has been recognized that a deep underground opening is more burst-prone when it approaches a geological discontinuity such as fault, dyke, and contact (Hedley et al., 1992; Snelling et al., 2013). Some studies have been conducted to explain the influence of structural planes on rockburst. For example, Zhang et al. (2013) conducted a numerical study that considered a fault near the drainage tunnel of the Jinping II hydropower station in China to explain a rockburst that occurred in the drainage tunnel. They showed that the presence of the fault near the tunnel could affect the rock failure. However, they could not estimate failure intensity (in terms of ejection velocity of broken rocks and released kinetic energy). In another study, Zhou et al. (2015) conducted some laboratory experiments to explore the role of weak planes on rockburst damage in tunnels. In their study, the role of weak planes on rockburst damage observed in the intake tunnels of the Jinping II hydropower station was explained by their observations from laboratory shear test results. They stated that weak planes could induce rockburst in tunnels with three possible mechanisms including fault-slip, shear rupture, and buckling. Manouchehrian (2016) used numerical models to study rockbursts near fault regions in deep tunnels. It shows in this study that weak planes around a tunnel may change the loading system stiffness of the failed rocks and induce rockbursts because when there is a weak plane near an underground opening, a large volume of rock is able to move more freely than that without a weak plane.

In this paper, the influence of geological weak planes on rockburst occurrence in tunnels that are subjected to static load increase and dynamic disturbance is investigated using Abaqus^{2D} explicit models. In Section 2, model responses between homogeneous and heterogeneous materials are studied. In Section 3, simulation of rockburst in tunnels without and with a nearby weak plane or fault is conducted. Static load increase and dynamic disturbance are considered in the models and the mechanism of rockburst in each loading condition is explained. A comparison of results between the models with and without a weak plane is also presented.

2. Rock failure simulation using Abaqus

Unstable rock failure is a dynamic phenomenon and should be treated as a nonlinear dynamic problem. Studies have shown that the explicit numerical method is more suitable than the implicit numerical method for solving nonlinear dynamic problems because the issue of convergence is eliminated. Abaqus is a FEM (finite element method)-based numerical tool which is equipped with implicit and explicit solvers, making it applicable for solving a large variety of physical and engineering problems (Dassault-Systems, 2010). Manouchehrian and Cai (2016a) simulated uniaxial and poly-axial compression tests using the Abaqus explicit tool and demonstrated the suitability of the tool for simulating unstable or dynamic rock failure. In this study, Abaqus explicit tool is used to simulate rockburst in deep tunnels.

A key characteristic of geomaterials is material heterogeneity, which cannot be readily modeled in Abaqus through GUI. Fortunately, Abaqus provides scripting capability for introducing material heterogeneity into models. In this section, a simulation of rock failure processes in compression using homogeneous material models is presented first, followed by a simulation of rock failure processes in compression using a heterogeneous material model.

2.1. Homogeneous model

To study rock failure using Abaqus, the laboratory tested mechanical parameters of T_{2b} marble (Table 1) are used as the base case. T_{2b} marble is the host rock of the diversion tunnels at the Jinping II hydropower station in China (Zhang et al., 2012).

Unconfined and confined compression tests are simulated to investigate the failure mechanism of homogeneous rocks. An elastoplastic Mohr-Coulomb strain-softening model with homogeneous material properties is used to model the strength of the T_{2b} marble. Table 2 presents the calibrated parameters for defining the strain-softening behavior of the rock in the homogeneous model. A rectangular specimen with a height of 250 mm and a width of 100 mm is used for simulation. A plane strain model is used. In the unconfined compression test simulation, one end of the specimen is fixed in the maximum stress direction and the other direction is free (roller constraint), and a constant velocity of 0.03 m/s is applied directly to the other end to load the specimen. The same end boundary conditions are applied to the specimens in the confined compression test simulations and the confinements applied are 5 MPa, 10 MPa, 20 MPa, and 40 MPa. In the developed homogeneous model, a uniaxial compressive strength (UCS) of 113.6 MPa, a friction angle of 30°, and a cohesion of 32.9 MPa are calculated, which are similar to the reported laboratory test data (Table 1).

Fig. 1 shows the failure pattern in the homogeneous models indicated by the plastic shear strain. The figure shows that confinement does not affect the failure patterns in the homogeneous model because all of them show distinct shear failure. Despite that the mechanical parameters of the T_{2b} marble are captured by the homogeneous model, it fails to capture the splitting failure under low confinement.

2.2. Heterogeneous model

In order to overcome the deficiency of the homogeneous models, Manouchehrian and Cai (2016b) introduced heterogeneity

Table 1
Physico-mechanical properties of the T_{2b} marble (Zhang et al., 2014).

Density, ρ (kg/m^3)	Young's modulus, E (GPa)	Poisson's ratio, ν	*UCS* (MPa)	Cohesion, c (MPa)	Friction angle, φ (°)	Post-peak modulus, E_{pp} (GPa)
2780	55	0.27	110.7[a]	32.6	29	150[b]

[a] UCS of the T_{2b} marble was reported between 100 MPa and 160 MPa in Zhang et al. (2014). This value was calculated according to $UCS = \frac{2c\cdot\cos\varphi}{1-\sin\varphi}$ for the present study.
[b] Post-peak modulus (E_{pp}) of the T_{2b} marble is extracted by digitizing curves presented in Zhang et al. (2014).

Please cite this article in press as: Manouchehrian A, Cai M, Analysis of rockburst in tunnels subjected to static and dynamic loads, Journal of Rock Mechanics and Geotechnical Engineering (2017), https://doi.org/10.1016/j.jrmge.2017.07.001

Table 2
Strain-softening parameters of the homogeneous model.

Cohesion		Tension cut-off	
Cohesion yield stress (MPa)	Shear plastic strain	Tension cut-off stress (MPa)	Tensile plastic strain
32.2	0	5.5	0
0.01	0.2	0.1	0.001

into Abaqus models. In the following simulation, the material properties E, c, and φ of each element were assigned randomly, following normal distribution functions. The coefficient of variation (COV) associated with each variable is 5%. The heterogeneous model was used to simulate the mechanical properties of the T_{2b} marble (Table 1). A UCS of 113.5 MPa, a friction angle of 29.7°, and cohesion of 32.7 MPa were estimated from the heterogeneous model, which were similar to the laboratory test results.

Fig. 1a shows the photographs of the failed T_{2b} marble specimens in laboratory tests (Zhang et al., 2014) and Fig. 1c presents the snapshots of the plastic strain obtained by numerical models. It is seen that in the heterogeneous model, the failure modes change from splitting failure at zero confinement to shear failure at high confinements. The homogeneous material models cannot capture axial splitting at zero confinement but the heterogeneous material model successfully captures this failure mode. Hence, the heterogeneous material model in Abaqus enhances its capability for solving geotechnical engineering problems.

3. Rockburst simulation

Tunnels in deep grounds are usually subjected to large static and dynamic loads. In this condition, tunnels are more prone to failure. Rockburst case histories have shown that rockburst can be triggered by either static load increase or dynamic disturbances

(a) Laboratory tests.

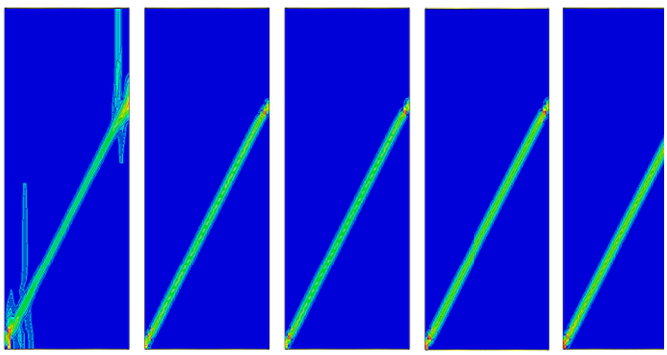

(b) Homogeneous model.

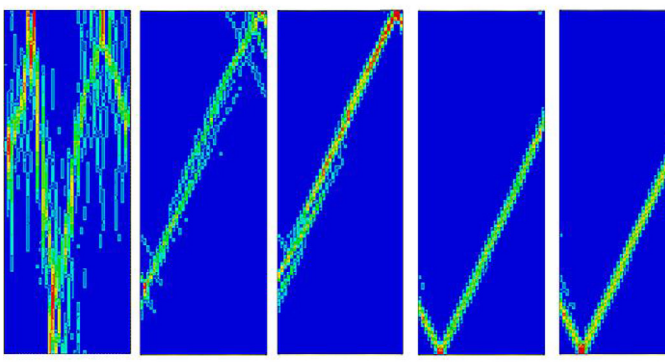

$\sigma_3 = 0$ MPa $\sigma_3 = 5$ MPa $\sigma_3 = 10$ MPa $\sigma_3 = 20$ MPa $\sigma_3 = 40$ MPa

(c) Heterogeneous model.

Fig. 1. Failure patterns at different confinements from (a) laboratory tests (Zhang et al., 2014), (b) homogeneous model, and (c) heterogeneous model (modified from Manouchehrian and Cai (2016b)).

Please cite this article in press as: Manouchehrian A, Cai M, Analysis of rockburst in tunnels subjected to static and dynamic loads, Journal of Rock Mechanics and Geotechnical Engineering (2017), https://doi.org/10.1016/j.jrmge.2017.07.001

(Salamon, 1983; Udd and Hedley, 1987; Young, 1993; Ortlepp and Stacey, 1994; Kaiser et al., 1996; Ortlepp, 1997; Andrieux et al., 2013). The possibility of rockburst occurrence is increased when a geological weak plane exists near a tunnel (Hedley, 1992). Being able to simulate rockburst triggered by static and dynamic loads is important for rock support design. In this paper, rockbursts in tunnels triggered by static load increase and dynamic disturbance are simulated.

3.1. Rockburst triggered by static load increase

In this section, models are developed to study the influence of weak planes on rockburst occurrence and damage numerically. A realistic simulation can be conducted using 3D (three-dimensional) models to study the stability of a long tunnel near geological structures. However, when the modeled weak plane near the tunnel is parallel to the tunnel axis, the problem can be treated as a 2D (two-dimensional) plane strain problem. A circular tunnel with a radius (r) of 5 m is modeled. In the numerical model, the outer boundary width and height are 15 times the tunnel diameter to exclude the effect of the outer boundary on stress redistribution around the tunnel (Fig. 2). In this study, the model also includes a fault with a varying length.

Before tunnel excavation, in situ stresses are applied to the outer boundaries and then the boundaries are fixed with roller constraints. Tunnel excavation is then simulated. The horizontal (σ_x) and vertical (σ_z) in situ stresses are assumed to be 30 MPa and 60 MPa, respectively. Gradual excavation of the tunnel is simulated by stress reduction at the tunnel boundary in ten steps. This simulates tangential stress increase due to tunnel advance.

An elastoplastic Mohr-Coulomb strain-softening model with heterogeneous material properties is used to model a rock mass with its physico-mechanical properties presented in Table 3. In the heterogeneous model, the mean values of E, c, and φ are 21 GPa, 22 MPa, and 31°, respectively, and the COVs of them are 5%. The parameters for defining the strain-softening behavior of the rock mass are presented in Table 4.

Firstly, a tunnel without any adjacent geological structure is modeled. Shear and tensile failures around the tunnel, indicated by the maximum principal plastic strains, are illustrated in Fig. 3. The figure shows a nearly symmetric failure around the tunnel, with

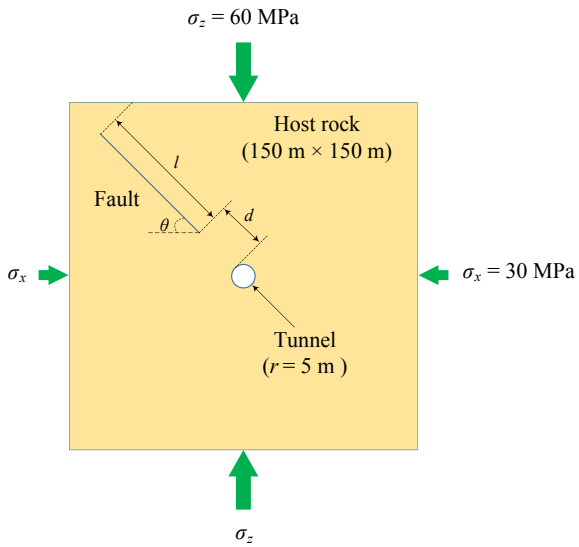

Fig. 2. Geometry and boundary conditions of the model subjected to static load.

Table 3
Rock mass physico-mechanical properties.

Density, ρ (kg/m^3)	Young's modulus, E (GPa)	Poisson's ratio, ν	UCS (MPa)	Cohesion, c (MPa)	Friction angle, φ (°)
2500	20	0.2	69.3	20	30

Table 4
Parameters with COV = 5% for defining the post-peak behavior of the rock mass.

Cohesion		Tension cut-off	
Cohesion yield stress (MPa)	Shear plastic strain	Tension cut-off stress (MPa)	Tensile plastic strain
22	0	3	0
0.01	0.2	0.01	0.005

shear failure zones located at 3 and 9 o'clock because the maximum in situ principal stress direction is vertical.

Fig. 4a shows the velocities of the element nodes around the tunnel at the beginning of Step 10 (at the time of failure). The figure shows a maximum velocity of 1.78 m/s in one node at the tunnel surface and the minimum velocity of the failed elements is 0.14 m/s. In this study, the velocities of all failed elements around the tunnel during the running time are tracked and then an average velocity (V_{max}) is calculated. The maximum of the average velocity ($\overline{V}_{max}$) during the running time is picked to interpret the results. In this case, the average of maximum velocity of the failed elements around the tunnel is $\overline{V}_{max}$ = 0.58 m/s. When failure is stable, the ejection velocity of the failed rocks is low (Milev et al., 2002). The maximum kinetic energy per unit volume (KE_{max}) of the failed rocks, which can be used as an indicator of rock failure intensity, is 0.65 kJ/m^3. Judged by the maximum of the average velocity and the maximum kinetic energy per unit volume, failure can be considered as stable in this case; if it were in the field, the failure would be in the form of spalling, spitting, or shallow slabbing.

Next, a fault with a dip of θ = 45°, a length of l = 80 m and at a position of d = 2.5 m from the tunnel wall is added to the model (see Fig. 2). A Coulomb model with a friction coefficient of 0.4 and zero cohesion is used to model the fault. It should be noted that the modeled fault is assumed to be straight and the fault's waviness that exists in reality is neglected. Therefore, interlocking between the two faces of the fault is not considered. This simplification makes the fault easier to slide. Hence, this model can be considered as an extreme case and the calculated $\overline{V}_{max}$ and KE_{max} are the upper bound values.

Development of rock failure around the tunnel as static stress increases, from Steps 1, 4, 9, to 10, is shown in Fig. 5. The figure

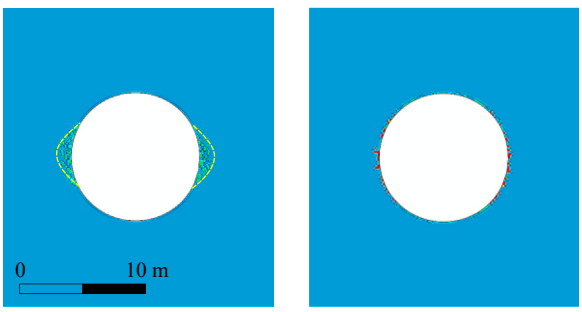

(a) Shear failure. (b) Tensile failure.

Fig. 3. Failure zones around the tunnel subjected to static load in the model without any nearby geological structures.

Please cite this article in press as: Manouchehrian A, Cai M, Analysis of rockburst in tunnels subjected to static and dynamic loads, Journal of Rock Mechanics and Geotechnical Engineering (2017), https://doi.org/10.1016/j.jrmge.2017.07.001

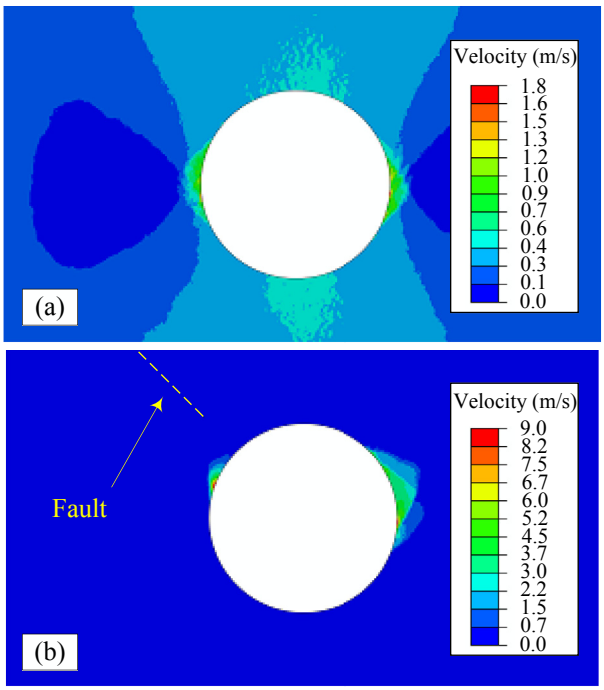

Fig. 4. Velocity distributions in the elements: (a) without and (b) with a nearby fault at the beginning of Step 10.

shows initiation of tensile and shear fractures at the tip of the fault at Step 1 excavation. Then, the shear fractures propagate toward the tunnel face (Step 4) and rocks between the fault and the tunnel are ruptured. Meanwhile, tensile fractures are initiated at the bottom of the tunnel. Slip of the fault due to excavation causes compression at positions of 1–4 o'clock (Step 9). At Step 10, the failed rocks on the right tunnel wall would blow out violently with a maximum velocity $\overline{V}_{max} = 3.4$ m/s (Fig. 5) and a failure pit with a depth of 3 m would be created. The maximum unit kinetic energy is 6.97 kJ/m^3.

Tunneling near a fault with different fault lengths is simulated to understand the influence of the fault length (l) on rockburst damage. The radius, r, of the circular tunnel is 5 m. The fault length (l) is varied at $l = 0$, 20, 40, 60, and 80 m, resulting in l/r ratios of 0, 4, 8, 12, and 16, respectively. The same modeling procedure described above is used.

The influence of l on $\overline{V}_{max}$ and KE_{max} is presented in Fig. 6. This figure indicates that an increase in the fault length results in increases of both $\overline{V}_{max}$ and KE_{max}. According to Fig. 6a, when $l = 0$ (i.e. there is no fault), $\overline{V}_{max}$ is low (0.58 m/s) and the rock failure can be considered as stable. $\overline{V}_{max}$ and KE_{max} increase rapidly as the l/r ratio increases. In Fig. 6, a trend change exists when l/r changes from 8 to 12. When the fault is longer (e.g. $l/r = 12$ and 16), its end is closer to the model boundary, and this can influence the results. The outside boundary width and height should be at least ten times the modeled structure to exclude the effect of the outer boundary on stress redistribution around the structure. In this study, in addition to the tunnel, a fault is included in the model. In this case, building a model that is large enough to exclude the boundary effect is computationally expensive. In Fig. 6, the dashed line may be used to correct the boundary effect. For example, for $l/r = 16$, we have $\overline{V}_{max} = 3.4$ m/s and $KE_{max} = 6.97$ kJ/m^3 from the modeling results, which can be modified to $\overline{V}_{max} = 2.2$ m/s and $KE_{max} = 2.8$ kJ/m^3 from the dashed line.

Fig. 7 shows the total displacement distribution around the tunnel at the end of Step 9 excavation (before the sidewall fails). This figure shows that when the fault is longer, a larger volume of hanging wall rocks can move toward the tunnel and push the rocks near the tunnel wall boundary, particularly the rocks on the right wall side. Hence, more strain energy release is possible if there is a sudden rock failure. This explains why the unit maximum kinetic energy is high for large l/r ratios. Furthermore, the displacement field also indicates that the mine system stiffness is low when the l/r ratio is high because the rocks surrounding the failed rocks can have more deformation.

The concept of mine system stiffness has been used by some researchers to explain rockburst in underground mines (Aglawe, 1999; Wiles, 2002). Although it is difficult to calculate mine system stiffness quantitatively in a tunnel setting, an analogy to the loading system stiffness in laboratory testing can be made. Laboratory test results show that the modes of failure (stable and unstable) depend on the relative stiffness of the rock and the loading

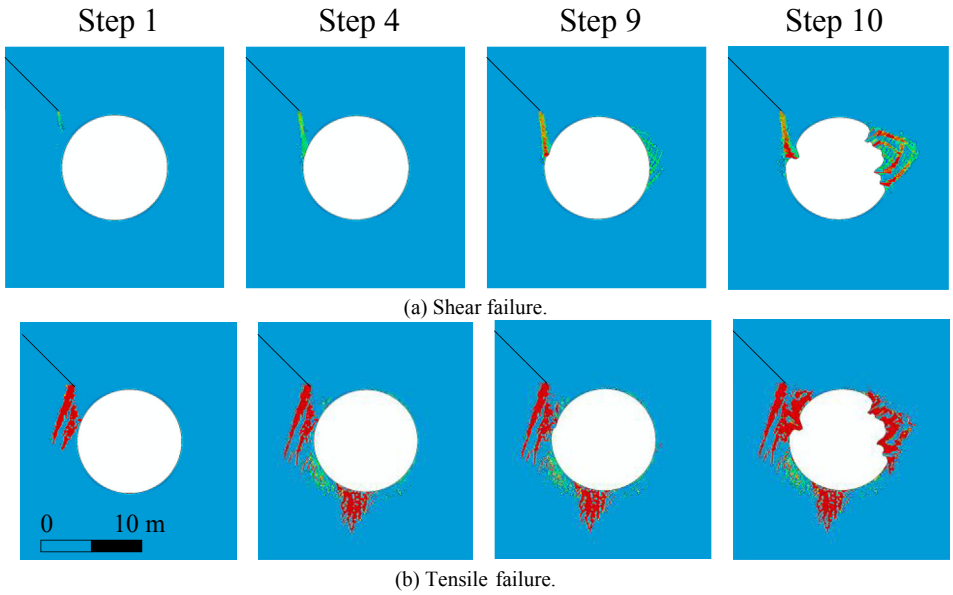

Fig. 5. Failure development around the tunnel with a nearby fault in various steps: (a) Shear failure, and (b) Tensile failure.

Please cite this article in press as: Manouchehrian A, Cai M, Analysis of rockburst in tunnels subjected to static and dynamic loads, Journal of Rock Mechanics and Geotechnical Engineering (2017), https://doi.org/10.1016/j.jrmge.2017.07.001

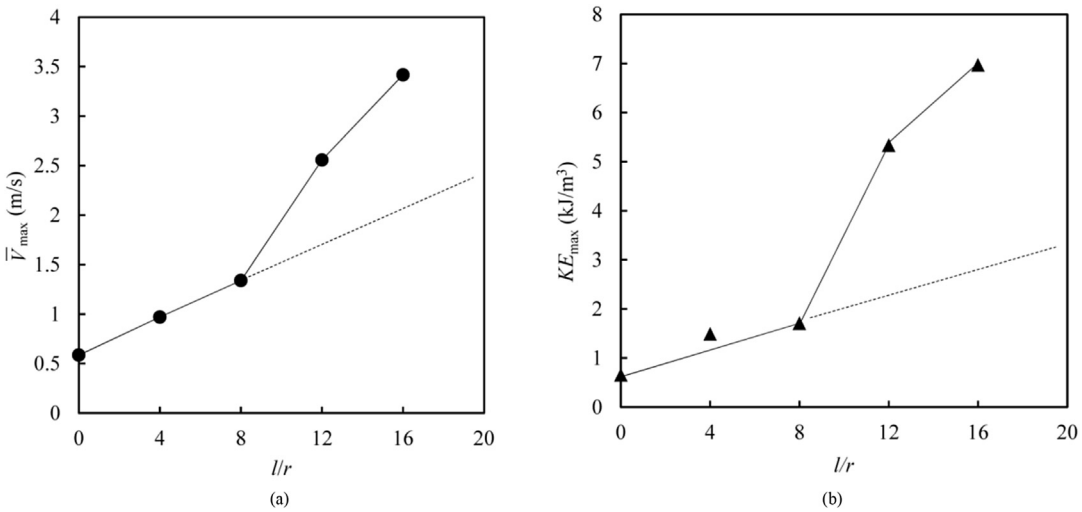

Fig. 6. Influence of fault length on (a) $\overline{V}_{max}$ and (b) KE_{max}. The black solid circles and triangles indicate numerical simulation results and the dash lines indicate trends of the data extending beyond $l/r = 0$ to 8.

system (Wawersik and Fairhurst, 1970). A soft loading system is capable of storing more strain energy than a stiff loading system. Thus, when a rock specimen fails, the failure is stable under a stiff loading system and unstable under a soft loading system. In spite of the loading condition difference in the field and in the laboratory, we can see that an increase of l decreases the mine system stiffness and as a result, unstable rock failure can occur around the tunnel. This can be clearly seen from the results presented in Figs. 6 and 7. Reduced mine system stiffness can be considered as a main effect of weak planes near openings in deep underground mines, which can potentially lead to rockburst (Manouchehrian, 2016).

3.2. Rockburst triggered by dynamic disturbance

Slab buckling has been identified as a mechanism of rockburst (Nemat-Nasser and Horii, 1982; Bardet, 1990; Ortlepp, 1993). Weak planes parallel to the tunnel boundaries and the maximum principal in situ stress may allow buckling type rockburst. When the rocks in a slab are highly stressed, a small increase of stress due to tunnel advance or dynamic disturbance from nearby blasting or a remote seismic event may trigger a rockburst.

Dynamic disturbance due to activities, such as explosion, vibration, and stress impact from nearby rockbursts, does influence

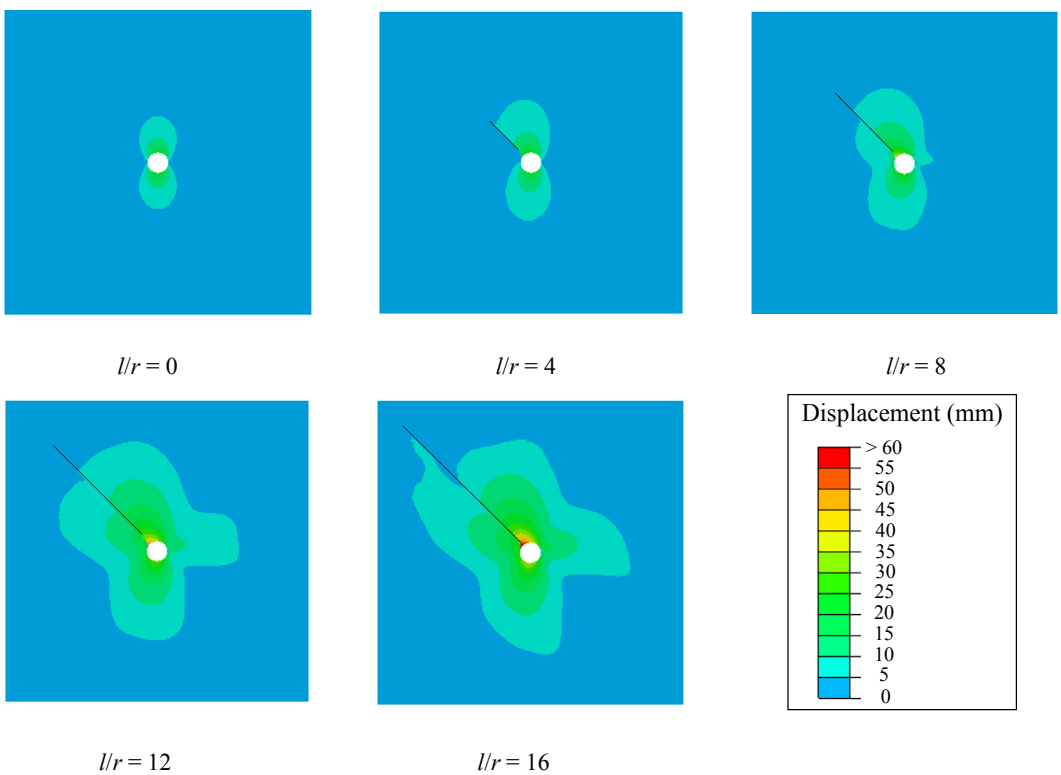

Fig. 7. Displacement around the tunnel in models with different fault lengths.

Please cite this article in press as: Manouchehrian A, Cai M, Analysis of rockburst in tunnels subjected to static and dynamic loads, Journal of Rock Mechanics and Geotechnical Engineering (2017), https://doi.org/10.1016/j.jrmge.2017.07.001

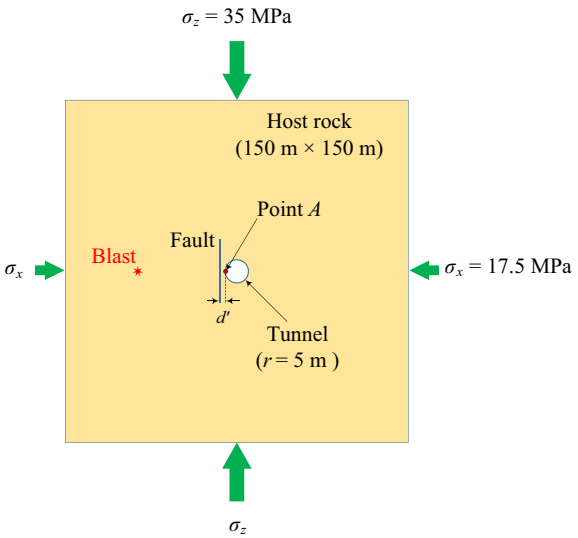

Fig. 8. Geometry and boundary conditions in the model subjected to dynamic disturbance.

rockburst damage. Studies have shown that external disturbances during underground mining can induce rockbursts (Blair, 1993; Kaiser et al., 1996; Zhu et al., 2010). In this section, the influence dynamic disturbance on rockburst occurrence near fault regions in deep tunnels is investigated. A circular tunnel with a radius of $r = 5$ m is considered. As shown in Fig. 8, the model size is 150 m × 150 m (width × height) and there is a fault near the tunnel at a distance of d'. The same elastoplastic Mohr-Coulomb strain-softening model used in Section 3.1 is used. The horizontal (σ_x) and vertical (σ_z) in situ stresses are assumed to be 17.5 MPa and 35 MPa, respectively to avoid any significant rock failure due to static load increase as a result of tunnel advance. Gradual excavation of the tunnel is simulated by stress reduction at the tunnel boundary in ten steps, using the modeling procedure explained in Section 3.1.

Dynamic disturbance in ground can be produced by different sources such as explosion, vibration, earthquake, and adjacent mining activities. Specific modeling techniques are needed to model different dynamic disturbances. In this study, it is assumed that the dynamic disturbance is generated due to blasting near the tunnel. In order to apply the blast load to the numerical model, a time history of load has to be defined. A blast hole with a radius of 0.5 m at a distance of 30 m away from the tunnel is generated in the model (Fig. 8), and then the blast load is applied to the blast hole wall (Fig. 9a). A triangular blast load function is selected (Fig. 9b). The peak stress of the compressive pulse and pulse duration are 200 MPa and 3 ms, respectively.

The model has a finite domain and quiet boundary conditions are often used to absorb the outward propagating waves. However, as the duration of the blasting is very short and the initial structure response is the major concern, boundaries can be set at a sufficient distance away from the tunnel and this will result in no reflected waves within the duration of interest or the amount of reflected waves is so small that it can be ignored (Yang and Hung, 1997). In the present study, the finite element model is large enough to avoid the influence of wave reflection on the modeling results. Fig. 10 illustrates the blast wave propagation (in terms of ground motion velocity) in a model without any geological structure. This figure shows that the reflected waves within the model running time (25 ms) do not reach the tunnel and hence will not affect the results.

Firstly, a tunnel without any adjacent geological structure is modeled. Because the stress level is lower than the rock strength, no failure occurs around the tunnel due to tunnel excavation. Then, the dynamic disturbance is applied to the model and the model response is recorded and analyzed. Fig. 11 illustrates the shear and tensile failures around the tunnel after the dynamic waves pass through the tunnel completely. Failure around the tunnel is in the form of small tensile fractures at the tunnel wall. Shear failure is not noticeable under this condition. Fig. 12 shows the ground motion velocity at a reference point at the position of 9 o'clock, indicated as "point A" in Fig. 8. The velocity drops to near zero as soon as the blast waves pass the tunnel. It should be noted that this velocity is the ground motion velocity, not the ejection velocity. The ground motion velocity distribution at $t = 15$ ms in the model without any geological structure is shown in Fig. 13a. At this time, the wave front has passed the tunnel and the ground motion velocity at the tunnel wall is very small.

Next, a vertical fault with a length of $l = 20$ m and at a distance of $d' = 0.5$ m from the tunnel wall is added to the model (see Fig. 8). A Coulomb model with a friction coefficient of 0.4 and zero cohesion

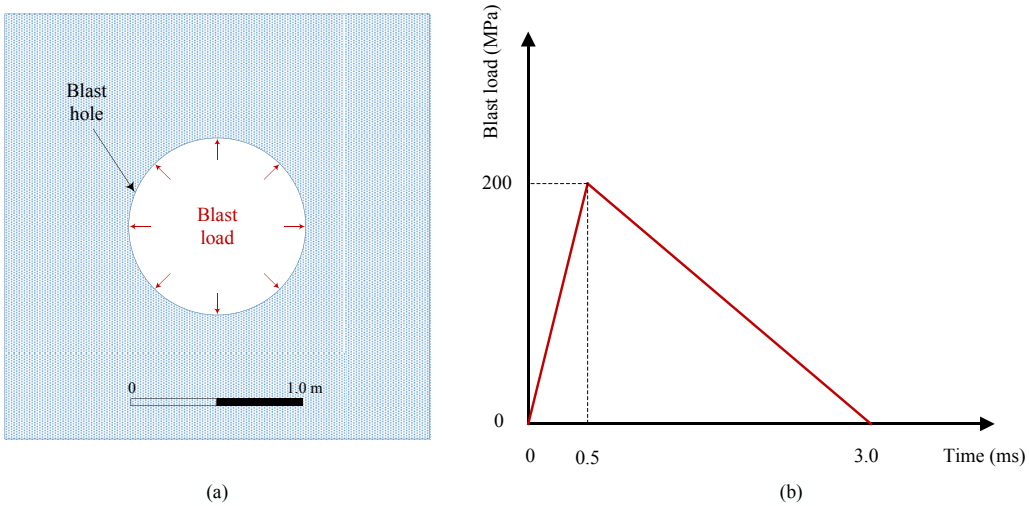

Fig. 9. (a) The blast hole and (b) the triangular blast load function.

Please cite this article in press as: Manouchehrian A, Cai M, Analysis of rockburst in tunnels subjected to static and dynamic loads, Journal of Rock Mechanics and Geotechnical Engineering (2017), https://doi.org/10.1016/j.jrmge.2017.07.001

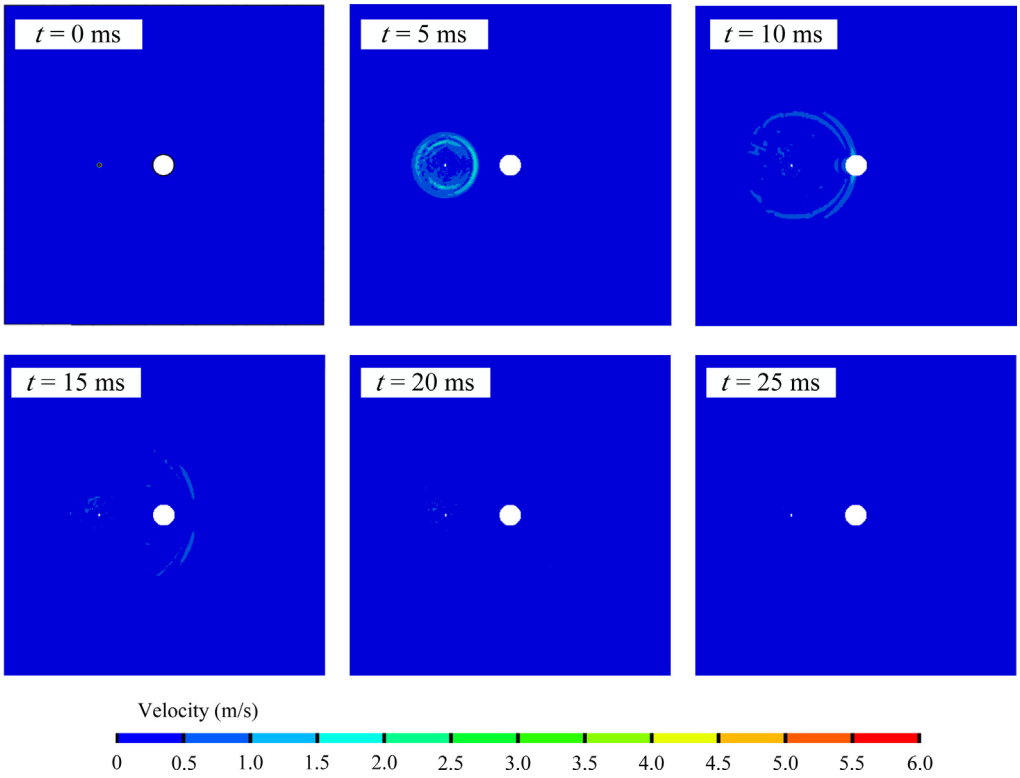

Fig. 10. Ground motion velocity distribution in a model without any geological structure.

is used to model the fault. Fig. 14 illustrates shear and tensile failures around the tunnel. Tensile fractures parallel to the tunnel wall are formed due to the blast wave. In addition, pushing action from the blast wave resulted in slab buckling and created some shear failures. The energy stored in the slab is released when failure occurs due to the slab flexure (Qiu et al., 2014). This energy is added to the amount of released energy due to failure at the tunnel wall and makes the failure more violent. However, the dominant failure mode under this condition is axial splitting. Fig. 12 indicates that the ground motion velocity at "point *A*" increases to 5.14 m/s after the blast wave passes the tunnel wall. It implies that the failed rocks might be ejected due to violent rock failure.

It can be understood from Figs. 11–14 that the rock failure is more violent if weak planes create slabs that are facing the incoming dynamic waves near the tunnel. When the rocks in the slabs are highly stressed, a small increase of stress due to tunnel advance or dynamic disturbance from nearby blasting or remote seismic events may trigger rockburst.

Tunneling near a fault with different blasting loads is simulated to understand the influence of blast load on rockburst damage. The blasting loads are varied at 100 MPa, 150 MPa, 200 MPa, and 250 MPa. The same modeling procedure described above is used. The influence of the blasting loads on the ground motion velocity at "point *A*" is illustrated in Fig. 15, showing that the ground motion velocity is higher when the blasting load is larger. This implies that rock failure triggered by large dynamic disturbance is more violent than that by smaller dynamic loads.

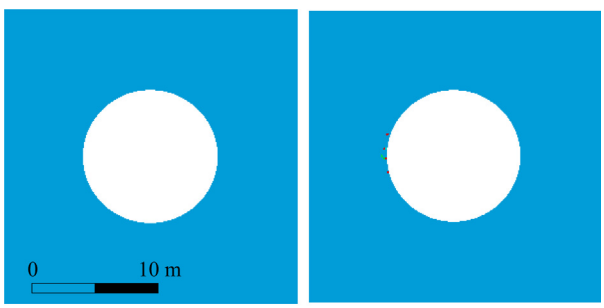

(a) Shear failure. (b) Tensile failure.

Fig. 11. Failure zones around the tunnel subjected to dynamic disturbance in the model without a nearby geological structure: (a) Shear failure, and (b) Tensile failure.

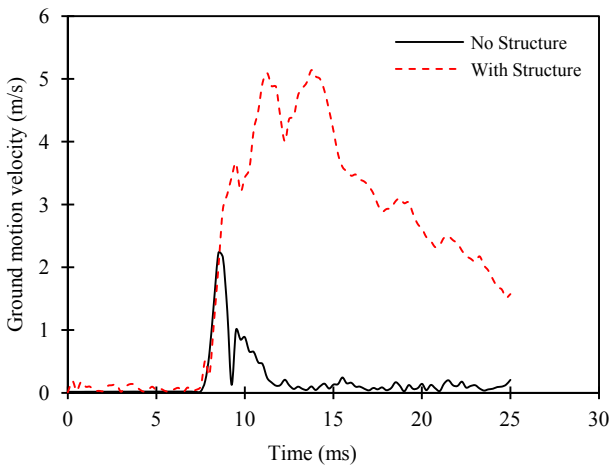

Fig. 12. Ground motion velocity at "point *A*" in the models with and without a geological structure.

Please cite this article in press as: Manouchehrian A, Cai M, Analysis of rockburst in tunnels subjected to static and dynamic loads, Journal of Rock Mechanics and Geotechnical Engineering (2017), https://doi.org/10.1016/j.jrmge.2017.07.001

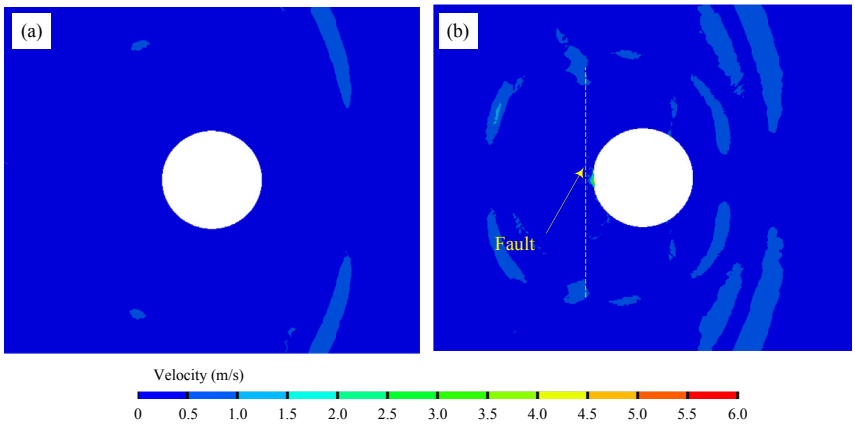

Fig. 13. Ground motion velocity at $t = 15$ ms in models (a) without and (b) with a geological structure.

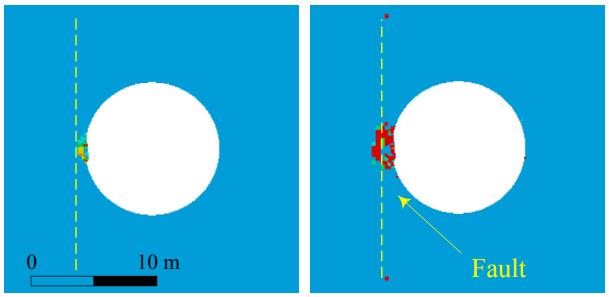

(a) Shear failure. (b) Tensile failure.

Fig. 14. Failure zones around the tunnel subjected to dynamic disturbance in the model with a nearby geological structure: (a) Shear failure, and (b) Tensile failure.

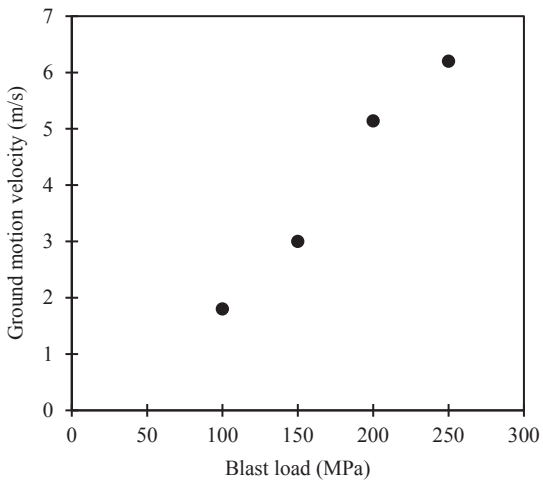

Fig. 15. Influence of blasting load on the ground motion velocity.

4. Conclusions

Rockburst is a challenging problem in deep underground mines and civil tunnels, which imposes a great danger on safety of personnel and investment. Many factors associated with rockburst damages have been identified and the presence of geological structures such as faults, shear zones, joints and dykes near excavation boundaries has been observed in many rockburst case histories but their role in rockburst occurrence is still not fully understood.

Rockbursts in tunnels with nearby geological structures under static and dynamic loads were studied using the Abaqus explicit code. Several tunnel models with and without faults were developed, and static and dynamic loads were applied. The peak particle velocity and the released kinetic energy of failed rocks, the failure zone around the tunnel, and the deformed mesh were studied to identify stable and unstable rock failures. When a weak plane was presented in the model, it resulted in more released kinetic energy and higher element velocity, indicating that rock failure became more violent. The modeling results also indicated that the failure became more violent when the weak plane was longer.

It shows that if weak planes near the tunnel are positioned parallel or sub-parallel to the tunnel wall, rock slabs are created which can change the failure mechanism at the tunnel wall. The energy stored in the slab is released when failure occurs due to the slab flexure, resulting in more released energy which in turn makes the failure more violent.

The approach presented in this study can capture dynamic response of a rock mass. In particular, it can estimate released kinetic energy and this can be useful for dynamic rock support design.

Conflict of interest

The authors wish to confirm that there are no known conflicts of interest associated with this publication and there has been no significant financial support for this work that could have influenced its outcome.

Acknowledgments

Financial supports from the Natural Sciences and Engineering Research Council (NSERC) of Canada (CRDPJ 418932-11), Vale, LKAB, CEMI, MIRARCO, and the Open Research Fund of the State Key Laboratory of Geomechanics and Geotechnical Engineering, Institute of Rock and Soil Mechanics, Chinese Academy of Sciences (Grant No. Z015001) for this work are gratefully acknowledged.

References

Aglawe J. Unstable and violent failure around underground openings in highly stressed ground. Ontario, Canada: Queen's University; 1999.

Andrieux P, Blake W, Hedley D, Nordlund E, Phipps D, Simser B, Swan G. Rockburst case histories: 1985, 1990, 2001 & 2013. Sudbury, Canada: CAMIRO Mining Division for the Deep Mining Research Consortium; 2013.

Please cite this article in press as: Manouchehrian A, Cai M, Analysis of rockburst in tunnels subjected to static and dynamic loads, Journal of Rock Mechanics and Geotechnical Engineering (2017), https://doi.org/10.1016/j.jrmge.2017.07.001

Bardet J. Numerical modeling of a rockburst as surface buckling. In: Proceedings of the 2nd international symposium on rockbursts and seismicity in mines, Minneapolis, 8–10 June 1988. Rotterdam: A.A. Balkema; 1990. p. 81–5.
Blair D. Blast vibration control in the presence of delay scatter and random fluctuations between blastholes. International Journal for Numerical and Analytical Methods in Geomechanics 1993;17(2):95–118.
Blake W, Hedley DG. Rockbursts: case studies from North American hard-rock mines. Littleton, Colorado: SME; 2003.
Cai M. Principles of rock support in burst-prone ground. Tunnelling and Underground Space Technology 2013;36(6):46–56.
Chen Z, Tang C, Huang R. A double rock sample model for rockbursts. International Journal of Rock Mechanics and Mining Sciences 1997;34(6):991–1000.
Dassault-Systems. Abaqus analysis user's manual. Dassault-Systems 2010.
Ghose AK, Rao HS. Rockbursts: global experiences. In: Papers presented at the 5th plenary scientific session of working group on rockbursts of international bureau of strata mechanics, February, 1988. Rotterdam: A.A. Balkema; 1990. p. 211.
Gibowicz SJ, Lasocki S. Rockbursts and seismicity in mines. In: Proceedings of the 4th international symposium on rockbursts and seismicity in mines, Krakow, Poland, 11–14 August 1997. Krakow, Poland: A.A. Balkema; 1997. p. 437.
He M, Miao J, Feng J. Rock burst process of limestone and its acoustic emission characteristics under true-triaxial unloading conditions. International Journal of Rock Mechanics and Mining Sciences 2010;47(2):286–98.
He M, Nie W, Zhao Z, Guo W. Experimental investigation of bedding plane orientation on the rockburst behavior of sandstone. Rock Mechanics and Rock Engineering 2012;45(3):311–26.
Hedley D. Rockburst handbook for Ontario hard rock mines. Ottawa, Canada. 1992.
Hedley DGF, Mineral CCF, Technology E, Association OM, Laboratories MR. Rockburst handbook for Ontario hardrock mines. Canada Center for Mineral and Energy Technology 1992.
Kaiser P, McCreath D, Tannant D. Rockburst support handbook. Geomechanics Research Centre, Laurentian University; 1996.
Kaiser PK, Cai M. Design of rock support system under rockburst condition. Journal of Rock Mechanics and Geotechnical Engineering 2012;4(3):215–27.
Li J, Fan P, Wang M. Failure behavior of highly stressed rocks under quasi-static and intensive unloading conditions. Journal of Rock Mechanics and Geotechnical Engineering 2013;5(4):287–93.
Li S, Feng XT, Li Z, Chen B, Zhang C, Zhou H. In situ monitoring of rockburst nucleation and evolution in the deeply buried tunnels of Jinping II hydropower station. Engineering Geology 2012;137–138:85–96.
Li X, Cao W, Zhou Z, Zou Y. Influence of stress path on excavation unloading response. Tunnelling and Underground Space Technology 2014;42:237–46.
Manouchehrian A. Numerical modeling of unstable rock failure. PhD Thesis. Laurentian University; 2016.
Manouchehrian A, Cai M. Simulation of unstable rock failure under unloading conditions. Canadian Geotechnical Journal 2016a;53(1):22–34.
Manouchehrian A, Cai M. Influence of material heterogeneity on failure intensity in unstable rock failure. Computers and Geotechnics 2016b;71:237–46.
Milev A, Spottiswoode S, Noble B, Linzer L, Van Zyl M, Daehnke A, Acheampong E. The meaningful use of peak particle velocities at excavation surfaces for the optimisation of the rockburst criteria for tunnels and stopes. SIMRAC Final Project Report GAP. 2002. p. 709.
Mitri H, Tang B, Simon R. FE modelling of mining-induced energy release and storage rates. Journal of the South African Institute of Mining and Metallurgy 1999;99(2):103–10.
Nemat-Nasser S, Horii H. Compression-induced nonplanar crack extension with application to splitting, exfoliation, and rockburst. Journal of Geophysical Research: Solid Earth 1982;87(B8):6805–21.
Ortlepp W. High ground displacement velocities associated with rockburst damage. In: Rockbursts and seismicity in mines. Rotterdam: A.A. Balkema; 1993. p. 101–6.
Ortlepp W, Stacey T. Rockburst mechanisms in tunnels and shafts. Tunnelling and Underground Space Technology 1994;9(1):59–65.
Ortlepp WD. Rock fracture and rockbursts: an illustrative study. South African Institute of Mining and Metallurgy 1997.
Qiu S, Feng X, Zhang C, Xiang T. Estimation of rockburst wall-rock velocity invoked by slab flexure sources in deep tunnels. Canadian Geotechnical Journal 2014;51(5):520–39.
Sainoki A, Mitri HS. Dynamic modelling of fault-slip with Barton's shear strength model. International Journal of Rock Mechanics and Mining Sciences 2014;67:155–63.
Salamon M. Rockburst hazard and the fight for its alleviation in South African gold mines. In: Rockbursts: prediction and control IMM. London; 1983. p. 11–36.
Shepherd J, Rixon L, Griffiths L. Outbursts and geological structures in coal mines: a review. International Journal of Rock Mechanics and Mining Sciences & Geomechanics Abstracts 1981;18(4):267–83.
Snelling PE, Godin L, McKinnon SD. The role of geologic structure and stress in triggering remote seismicity in Creighton mine, Sudbury, Canada. International Journal of Rock Mechanics and Mining Sciences 2013;58:166–79.
Sun JS, Zhu QH, Lu WB. Numerical simulation of rock burst in circular tunnels under unloading conditions. Journal of China University of Mining and Technology 2007;17(4):552–6.
Tao M, Li X, Wu C. Characteristics of the unloading process of rocks under high initial stress. Computers and Geotechnics 2012;45:83–92.
Udd JE, Hedley D. Rockburst research in Canada-1987. In: Proceedings of the 6th ISRM congress, 30 August–3 September. Montreal, Canada: International Society for Rock Mechanics; 1987.
Wawersik W, Fairhurst C. A study of brittle rock fracture in laboratory compression experiments. International Journal of Rock Mechanics and Mining Sciences & Geomechanics Abstracts 1970;7(5):561–75.
Whyatt J, Blake W, Williams T, White B. 60 years of rockbursting in the Coeurd'Alene district of Northern Idaho, USA: lessons learned and remaining issues. In: Presentation at 109th annual exhibit and meeting. Phoenix: Society for Mining, Metallurgy, and Exploration; 2002. p. 25–7.
Wiles T. Loading system stiffness-a parameter to evaluate rockburst potential. In: First international seminar on deep and high stress mining. Perth, Australia: Australian Centre for Geomechanics; 2002.
Xiao Y, Feng X, Li S, Feng G, Yu Y. Rock mass failure mechanisms during the evolution process of rockbursts in tunnels. International Journal of Rock Mechanics and Mining Sciences 2016;83:174–81.
Yang YB, Hung HH. A parametric study of wave barriers for reduction of train-induced vibrations. International Journal for Numerical Methods in Engineering 1997;40(20):3729–47.
Young RP. Rockbursts and seismicity in mines 93. In: Proceedings of the 3rd international symposium, Kingston, Ontario, 16–18 August 1993. Kingston, Canada: Taylor & Francis; 1993. p. 462.
Zhang C, Feng XT, Zhou H, Qiu S, Wu W. Case histories of four extremely intense rockbursts in deep tunnels. Rock Mechanics and Rock Engineering 2012;45(3):275–88.
Zhang C, Feng XT, Zhou H, Qiu S, Wu W. Rockmass damage development following two extremely intense rockbursts in deep tunnels at Jinping II hydropower station, Southwestern China. Bulletin of Engineering Geology and the Environment 2013;72(2):237–47.
Zhang C, Feng XT, Zhou H, Qiu S, Yang Y. Rock mass damage induced by rockbursts occurring on tunnel floors: a case study of two tunnels at the Jinping II hydropower station. Environmental Earth Sciences 2014;71(1):441–50.
Zhao XG, Cai M. Influence of specimen height-to-width ratio on the strainburst characteristics of Tianhu granite under true-triaxial unloading conditions. Canadian Geotechnical Journal 2014;52(7):890–902.
Zhou H, Meng F, Zhang C, Hu D, Yang F, Lu J. Analysis of rockburst mechanisms induced by structural planes in deep tunnels. Bulletin of Engineering Geology and the Environment 2015;74(4):1435–51.
Zhu QH, Lu WB, Sun JS, Yi L, Ming C. Prevention of rockburst by guide holes based on numerical simulations. Mining Science and Technology (China) 2009;19(3):346–51.
Zhu WC, Li ZH, Zhu L, Tang CA. Numerical simulation on rockburst of underground opening triggered by dynamic disturbance. Tunnelling and Underground Space Technology 2010;25(5):587–99.
Zhu WS, Yang WM, Li XJ, Xiang L, Yu DJ. Study on splitting failure in rock masses by simulation test, site monitoring and energy model. Tunnelling and Underground Space Technology 2014;41:152–64.
Zipf RK. Simulation of cascading pillar failure in room-and-pillar mines using boundary-element-method. In: The 2nd North American rock mechanics symposium. American Rock Mechanics Association; 1996. ARMA-96–1887.

Amin Manouchehrian obtained his Bachelor's degree in Mining Engineering from Yazd University (Iran) in 2008 and his Master's degree in Mining Engineering/Rock Mechanics from Sahand University of Technology (Iran) in 2010. He joined Yazd University's Geomechanic Research Group in 2011 as a Research Engineer, where he involved in researching on "crack propagation mechanism under various loading conditions". He received his PhD degree in Mining Engineering/Rock Mechanics from Laurentian University (Canada) in 2016. Amin's recent research interest has been on the application of finite element method for rockburst modeling in deep tunnels which constitutes his PhD research work at Laurentian University.

Dr. Ming Cai is a full professor and Geomechanics Research Chair in the Bharti School of Engineering, Laurentian University, Canada. He obtained his Bachelor and Master's degrees from Tsinghua University in Beijing, China and his PhD in 1992 from the University of Tokyo, Japan. He is a registered Professional Engineer in Ontario, Canada, an editorial member of *International Journal of Georesources and Environment* (IJGE), *Tunnelling and Underground Space Technology*, *Rock Mechanics and Rock Engineering*, and *Canadian Geotechnical Journal*. He is the author and co-author of more than 150 scientific publications and the inventor of 4 patents.

Please cite this article in press as: Manouchehrian A, Cai M, Analysis of rockburst in tunnels subjected to static and dynamic loads, Journal of Rock Mechanics and Geotechnical Engineering (2017), https://doi.org/10.1016/j.jrmge.2017.07.001